Experimental Neurology 374 (2024) 114716

Contents lists available at ScienceDirect

Experimental Neurology

journal homepage: www.elsevier.com/locate/yexnr

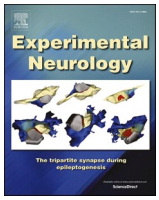

Research paper

Changes in glial cell activation and extracellular vesicles production precede the onset of disease symptoms in transgenic hSOD1^{G93A} pigs

Maria Teresa Golia [a], Roberto Frigerio [b,1], Susanna Pucci [a,1], Francesca Sironi [c], Cassandra Margotta [c], Laura Pasetto [c], Camilla Testori [d], Elena Berrone [d], Francesco Ingravalle [d], Marcella Chiari [b], Alessandro Gori [b], Roberto Duchi [e], Andrea Perota [e], Luca Bergamaschi [e], Antonio D'Angelo [f], Giulia Cagnotti [f], Cesare Galli [e], Cristiano Corona [d], Valentina Bonetto [c], Caterina Bendotti [c], Marina Cretich [b,2], Sara Francesca Colombo [a,2], Claudia Verderio [a,*,2]

[a] National Research Council of Italy, Institute of Neuroscience (IN-CNR), Via Raoul Follereau 3, 20854 Vedano al Lambro, Italy
[b] National Research Council of Italy, Institute of Chemical Science and Technologies (SCITEC-CNR), Via Mario Bianco 9, 20131 Milan, Italy
[c] Research Center for ALS, Istituto di Ricerche Farmacologiche Mario Negri IRCCS, Via Mario Negri, 2, 20156 Milano, Italy
[d] Istituto Zooprofilattico Sperimentale del Piemonte Liguria e Valle d'Aosta (IZSPLV), Via Bologna 148, 10154 Torino, Italy
[e] Avantea, Laboratory of Reproductive Technologies, Via Porcellasco 7/F, 26100 Cremona, Italy
[f] Department of Veterinary Sciences, University of Turin, Largo Paolo Braccini 2, 10095 Grugliasco, Torino, Italy

ARTICLE INFO

Keywords:
hSOD^{G93A} swine model
Extracellular vesicles
Biological fluids
Disease biomarkers

ABSTRACT

SOD1 gene is associated with progressive motor neuron degeneration in the familiar forms of amyotrophic lateral sclerosis. Although studies on mutant human SOD1 transgenic rodent models have provided important insights into disease pathogenesis, they have not led to the discovery of early biomarkers or effective therapies in human disease. The recent generation of a transgenic swine model expressing the human pathological hSOD1^{G93A} gene, which recapitulates the course of human disease, represents an interesting tool for the identification of early disease mechanisms and diagnostic biomarkers. Here, we analyze the activation state of CNS cells in transgenic pigs during the disease course and investigate whether changes in neuronal and glial cell activation state can be reflected by the amount of extracellular vesicles they release in biological fluids. To assess the activation state of neural cells, we performed a biochemical characterization of neurons and glial cells in the spinal cords of hSOD1^{G93A} pigs during the disease course. Quantification of EVs of CNS cell origin was performed in cerebrospinal fluid and plasma of transgenic pigs at different disease stages by Western blot and peptide microarray analyses. We report an early activation of oligodendrocytes in hSOD1^{G93A} transgenic tissue followed by astrocyte and microglia activation, especially in animals with motor symptoms. At late asymptomatic stage, EV production from astrocytes and microglia is increased in the cerebrospinal fluid, but not in the plasma, of transgenic pigs reflecting donor cell activation in the spinal cord. Estimation of EV production by biochemical analyses is corroborated by direct quantification of neuron- and microglia-derived EVs in the cerebrospinal fluid by a Membrane Sensing Peptide enabled on-chip analysis that provides fast results and low sample consumption. Collectively, our data indicate that alteration in astrocytic EV production precedes the onset of disease symptoms in the hSOD^{G93A} swine model, mirroring donor cell activation in the spinal cord, and suggest that EV

Abbreviations: AChR-g, acetylcholine receptor g-subunit; ALS, Amyotrophic lateral sclerosis; ALDH1L1, aldehyde dehydrogenase 1 family member L1; AnnxA2, Annexin-A2; BBB, blood-brain barrier; CD171, neural cell adhesion molecule L1; CNPase, cyclic nucleotide 3′-phosphodiesterase; CNS, central nervous system; CSF, cerebrospinal fluid; EVs, extracellular vesicles; EXOQ, ExoQuick Exosome Precipitation Solution; GFAP, Glial Fibrillary Acidic Protein; GPR17, G protein-coupled receptor 17; GST-π, glutathione-S-transferase-pi; hSOD, human SOD1; MAP2, Microtubule-Associated Protein 2; MOG, myelin-oligodendrocyte glycoprotein; MSP, membrane sensing peptide; NFL, Neurofilament light chain; NG2, Neural/glial antigen 2; NTA, Nanoparticle Tracking Analysis; OPC, oligodendrocyte progenitor cells; PBS, phosphate-buffered saline; PDGFR-a, Platelet-Derived Growth Factor Receptor Alpha; PLP1, Proteolipid protein 1; PTX3, pentraxin-3; SOD1, Cu/Zn superoxide dismutase 1; SP-IRIS, Single Particle Interferometric Reflectance Imaging Sensor; swSOD1, swine SOD1; Tg, transgenic; TRPS, Tunable Resistive Pulse Sensing; TMEM119, Transmembrane protein 119; Tub b3, Tubulin β3; WB, Western blot; Wt, Wild-type..

* Corresponding author at: National Research Council of Italy, Institute of Neuroscience (IN-CNR), Via Raoul Follereau 3, 20854 Vedano al Lambro, Italy.
E-mail address: c.verderio@in.cnr.it (C. Verderio).

[1] These authors equally contributed to this manuscript.
[2] These authors equally contributed to this manuscript.

https://doi.org/10.1016/j.expneurol.2024.114716
Received 13 October 2023; Received in revised form 23 January 2024; Accepted 4 February 2024
Available online 6 February 2024

measurements from the cells first activated in the ALS pig model, *i.e.* OPCs, may further improve early disease detection.

1. Introduction

Amyotrophic lateral sclerosis (ALS) is an adult-onset neurodegenerative disease characterized by loss of motor neurons in the motor cortex, brainstem, and spinal cord. It is a rare and fatal disorder that leads to muscle atrophy and weakness resulting in progressive paralysis and death from respiratory failure, typically within a few years after symptom onset (Hardiman et al., 2017). Cu/Zn superoxide dismutase 1 (SOD1) has been the first and most studied gene causative for familiar forms of ALS (Rosen et al., 1993). The identification of pathogenic SOD1 mutations in ALS patients has led to the generation of mutant human SOD1 transgenic (Tg) rodent models, which replicate key features of the disease (Turner and Talbot, 2008). Although these Tg models have provided important insights into the disease pathogenesis and potential treatments (Philips and Rothstein, 2015), they have so far been largely ineffective in targeting early pathological mechanisms of human disease and therapeutic intervention are administered relatively late in the disease course (Benatar et al., 2022). One of the possible reasons limiting translational research could be anatomical, physiological, and genetic differences between species. Thus, large animals like pigs, which share anatomical, physiological, and pathophysiological similarities with humans (Schomberg et al., 2016) have recently been used for modelling ALS (Yang et al., 2014; Chieppa et al., 2014). In a previous work, it has been found that Tg pig expressing the human pathological hSOD1^{G93A} gene displays several pathological features of ALS patients such as motor neuron degeneration, gliosis and hSOD1 protein aggregates in the brainstem and spinal cord (Crociara et al., 2019). Interestingly, unlike mouse models, hSOD1^{G93A} Tg pig recapitulated the human disease course with a long pre-symptomatic period before the onset of clinical symptoms (Crociara et al., 2019; Talbot, 2014). This suggested that swine model may represent a tool to identify pre-symptomatic diagnostic biomarkers and help in early therapy.

Extracellular vesicles (EVs) are heterogeneous cell-derived membranous particles that can be classified as endosome-derived small exosomes or medium-large plasma membrane-derived microvesicles according to their biogenesis pathways and size (Doyle and Wang, 2019). EVs are released by most cell types, including brain cells (neurons, astrocytes, microglia and oligodendrocytes) (Fauré et al., 2006; Krämer-Albers et al., 2007; Bianco et al., 2005) and are important mediators of cell-to-cell communication (Maas et al., 2017; Basso and Bonetto, 2016). By carrying and transferring a wide variety of bioactive molecules (nucleic acids, proteins, and lipids) between cells, EVs play crucial functions in both healthy and diseased brain. EV production increases from neurons and glial cells in response to physiological stimuli (neurotransmitters), danger/inflammatory signals (Fauré et al., 2006; Lachenal et al., 2011; Gabrielli et al., 2022) or stress conditions (Cai et al., 2018; Janas et al., 2016; Chiaradia et al., 2021). Importantly, the composition of brain cell-derived EVs also changes reflecting the activation state and phenotype of parental cells. For example, under neurodegenerative diseases, pathogenic proteins including ALS-causative mutant proteins (SOD1 and TDP-43) can become part of the EV cargo (Coleman and Hill, 2015; Silverman et al., 2016; Ferrara et al., 2018). Once released, EVs interact and signal to adjacent brain cells. Alternatively, EVs cross the blood-brain barrier (BBB) and spread into biofluids, including cerebrospinal fluid (CSF) and plasma, to reach and signal to distant cells (Saint-Pol et al., 2020), especially in pathological conditions promoting BBB leakage. Hence, quantification and phenotyping of EVs of different brain cell origin in biological fluids may provide valuable information on the state of parental cells, contributing to the discovery of disease biomarkers.

The development of methods for isolation and quantification of brain cell-derived EVs in biofluids is constantly advancing. However, analysis of the absolute number and size of EVs isolated by this two-step procedure is still challenging when performed by classical methodologies, such as Nanoparticle Tracking Analysis (NTA) or Tunable Resistive Pulse Sensing (TRPS), which cannot distinguish EVs from possible contaminants such as lipoproteins or protein aggregates generated during the isolation/elution procedure (Ekström et al., 2022). Developing a method for direct phenotyping and quantification of EVs in CSF, without previous steps of EV isolation/elution will limit possible artifacts and provide faster EV measurements, thus increasing the diagnostic potential of brain derived EVs in preclinical and clinical contexts.

Here, we performed a biochemical characterization (phenotyping) of neurons and glial cells (astrocytes, oligodendrocytes, and microglia) in the spinal cord of hemizygous hSOD1^{G93A} transgenic pigs, expressing multiple copies of human hSOD1^{G93A} gene, at asymptomatic and symptomatic stages compared to age-matched Wild type (Wt) animals. In addition, by Western blot (WB) analysis and the use of brain cell lineage markers, present at EV surface or in their lumen, we measured the amount of EVs of neuronal and glial origin in the CSF as an index of cell activation and/or exposure to stressful conditions at all disease stages. Results of this analysis were then used to validate a new method for direct measurements of neuron- and microglia-derived EVs directly in the CSF by peptide microarrays and Single Particle Interferometric Reflectance Imaging Sensor (SP-IRIS) platform using the ExoView instrumentation (now Unchained Lab) and chips spotted with a Membrane Sensing Peptide (MSP) (Gori et al., 2020).

2. Materials and methods

2.1. Animals

All procedures were conducted as described by the institutional guidelines that are in accordance with national (D.L. no. 116, G.U. suppl. 40, February 18, 1992, no. 8, G.U., 14 luglio 1994; D.L.26/2014) and international laws and policies (EEC Council Directive 86/609, 63/2010, OJ L 358, December 12, 1987; National Institutes of Health Guide for the Care and Use of Laboratory Animals, US National Research Council, 1996). Hemizygous hSOD1^{G93A} transgenic pigs were produced as previously reported (Chieppa et al., 2014). The study protocol was approved by the local ethics committee (Prot. N. 1043/2016-PR and N. 1187/2020-PR). The study included a total of 16 hSOD1^{G93A} Tg pigs and 16 Wt animals. Based on age, Tg pigs were divided into three study groups and matched with the relative controls. To investigate the preclinical phase of the disease, Tg pigs were sacrificed at an early and late asymptomatic stage when the animals reached 8–17 months and 22–26 months, respectively. Symptomatic Tg animals were sacrificed after the onset of clinical symptoms at 35–43 months. Clinical features of Tg and Wt pigs are reported in Table 1A and B, respectively.

2.2. Clinical, neurological and pathological examination

Clinical observation and physical assessment of animals were carried out daily by the animal husbandry staff and the veterinarian. Neurologic examination was performed monthly by a board-certified neurologist. For this purpose, a clinical examination protocol was properly developed and adapted to the swine species. The protocol followed the standard procedure for assessing mental status, posture, gait, and, when feasible, cranial nerves. Information on proprioception and postural reactions as well as spinal reflexes were deducted from the posture and gait analysis.

Onset and survival curves were performed using Kaplan–Meier

analyses. Disease onset was determined when animals consistently showed at least two of the following clinical signs: abnormal mental status/behaviour, abnormal gait and posture, respiratory distress, and dysphagia. Endpoint was defined as the death point when animals became inappetent or tended toward recumbency.

To evaluate the extent of muscle denervation, the expression level of acetylcholine receptor γ-subunit (AChR-γ) mRNA was examined in the diaphragm obtained from autopsy of the pigs at different stage of the disease. We have recently demonstrated that this parameter reflects the degree of denervation as measured by electromyography in ALS mouse models (Margotta et al., 2023).

2.3. REAL-TIME PCR analysis

RNA from pig diaphragm muscle was extracted using Trizol (Invitrogen) and purified with PureLink RNA columns (Life Technologies). RNA samples were treated with DNase I, and reverse transcription was performed with High-Capacity cDNA Reverse Transcription Kit (Life Technologies). Real-time PCR was performed using the TaqMan Gene expression assay (Applied Biosystems) following the manufacturer's instructions, on cDNA specimens in triplicate, using 1× Universal PCR Master Mix (Life Technologies) and 1× mix containing specific receptors probes (Life Technologies). Relative quantification was calculated from the ratio between the cycle number (Ct) at which the signal crossed a threshold set within the logarithmic phase of the given gene and that of the reference GAPDH gene (Ss03375435_u1; Life Technologies). Mean values of the triplicate results for each animal were used as individual data for 2-ΔCt statistical analysis. The following is the list of probes used: nicotinic cholinergic receptor, gamma subunit (Ss06860579_g1; Life Technologies).

2.4. Neurofilament light chain (NFL) analysis

NFL concentration was measured in CSF and serum using the Simoa® NF-light™ Advantage kit (No. 103400) on the Quanterix SR-X™ platform (Quanterix Corp, Boston, MA, USA). CSF (diluted 1:100) and serum (diluted 1:4) were analyzed following the manufacturer's instructions.

2.5. Spinal cord sampling and homogenates preparation

Pigs were sacrificed according to the approved protocol of animal welfare. Spinal cords were rapidly dissected out, precooled in isopentane and frozen in liquid nitrogen. Transverse frozen sections of spinal cords cervical tracts were sliced, and then homogenized with the help of a tissue grinder Potter-Elvehjem in cold phosphate-buffered saline (PBS); 100 mg tissue/mL buffer) plus protease inhibitors pepstatin (5 μg/mL), bestatin (5 μg/mL), aprotinin (5 μg/mL) and phenylmethylsulfonyl fluoride (PMSF; 2 mM) (Merck, Darmstadt, Germany).

2.6. CSF, plasma and serum sampling

Pigs were anesthetized with a KTX mixture (ketamine, tiletamine, xylazine, 1 mL per 15 kg of body weight).

CSF was obtained by lumbo-sacral puncture with the animals in sternal recumbency. After cleaning and disinfecting of the area, 5–10 ml of CSF per animal were collected using a spinal needle of 18G for 6 in. CSF samples were stored in plain tubes, immediately centrifuged at 2000 x*g* for 10 min at 4 °C and carefully inspected for the absence of a red blood cell pellet before to be stored at −80 °C in aliquots.

Blood sampling was performed with the animal in dorsal recumbency by puncturing the jugular vein. Whole blood was collected in commercially silica-treated (Vacutainer SST Advance; REF N° 366,468; BD Plymouth, UK) and in anticoagulant-treated (EDTA; Vacutainer K2E; REF N° 367,525; BD, Plymouth, UK) tubes. Resulting samples were inverted 8 times. Clotting was achieved in. serum tubes after 30 min at room temperature before their first centrifugation (2500 *g* × 15 min at +4 °C). Instead, plasma tubes were immediately processed (2500 g × 15 min at 4 °C). Obtained serum or plasma fractions were finally transferred in new clean tubes. Cells were then removed from serum or plasma by centrifugation for 15 min at3,000 x*g* using a refrigerated centrifuge. All samples were then stored at −80 °C in aliquots until further analysis.

2.7. EV isolation from body fluids

Aliquots of clean (no red cells in pellet) supernatants (2.6 ml) were used for direct EV measurements of particle concentration and size (100 μl for TRPS; 500 μl for NTA) while the remaining supernatant (2 ml) was ultracentrifuged at 100,000 ×g for 1 h at 4 °C (Beckman TL-100 / TL100 Optima Ultracentrifuge, rotor TLA100.3) to isolate both large and small EVs for WB analysis. The EV pellets were resuspended with Laemmli buffer and frozen until use.

EVs isolation from plasma was performed with ExoQuick Exosome Precipitation Solution (EXOQ; System biosciences, SBI, Palo Alto, CA, USA) following the manufacturer's protocol. Briefly, 500 μl of plasma samples was centrifugated at 3000 ×g for 15 min to remove any cells and debris. 250 μl of supernatant was then incubated for 30 min at 4 °C with 67 μl of EXOQ and centrifuged at 3000 ×*g* for 10 min at RT to pellet small EVs. EV pellets were resuspended in 200 μl of Buffer B and add 200 μl of Buffer A, the purification column was washed, and the sample

Table 1
Clinical features of **A)** hSOD1^{G93A} Tg pigs and **B)** age-matched Wt animals. HE: Euthanasia on Health indicate pigs which were sacrificed before overt clinical symptoms; M: male; F: female.

A	Tg pigs ID	Sex	Age at onset (months)	Age at sacrifice (months)	Clinical signs	B	Wt pigs ID	Sex
	448	F	HE	8.7	HE		405	M
	447	F	HE	8.7	HE		406	M
	450	F	HE	9.37	HE		404	F
	451	F	HE	10.03	HE		331	F
	329	F	HE	14.17	HE		408	M
Early	360	M	HE	15.50	HE		358	F
Asymptomatic	359	F	HE	16.97	HE		363	F
						Age-matched	279	M
	200	F	HE	22.17	HE		306	M
	282	M	HE	24.90	HE		304	M
	283	F	HE	25.87	HE		187	M
LateAsymptomatic	285	F	HE	25.87	HE	**Age-matched**	188	F
	20	M	35.03	35.50	Motor deficits and labored breathing		91	F
	21	M	35.83	36.17	Labored breathing		24	M
	26	M	38.20	38.43	Sudden death due to acute respiratory failure after sedation		787	M
	27	M	42.47	42.87	Sudden death due to acute respiratory failure after sedation		25	M
Symptomatic	23	M	42.47	42.90	Motor deficits and labored breathing	**Age-atched**		

loaded for EV isolation. EVs were resuspended with Laemmli buffer and frozen for WB analysis.

2.8. Tunable resistive pulse sensing analysis

TRPS analysis was made on all clean CSF and plasma samples with the qNano instrument (Izon, Christchurch, New Zealand) which provides size and concentration measurements of EVs by detecting current blockage from EVs passing through a polyurethane nanopore membrane NP200 (85–500 nm diameter range). 0.1 μm-filtered PBS supplemented with 0.3% Wetting Solution (from Izon EV reagent kit), was used to pretreat the pore in order to prevent EVs binding to the pore or spontaneous EV aggregation. Calibration measurements using 200 nm carboxylated polystyrene beads (supplied by Izon and diluted following the manufacturer's instructions) were performed immediately before and/or after the experimental samples at the same system setting. Data acquisition and analysis were performed using Izon Control Suite software (version V3.4). TRPS was used to measure concentration, size distribution and mode of EVs in 30 μl of undiluted pre-cleaned CSF sample. EVs quantification is described per ml. All recording were performed in duplicate.

2.9. Nanoparticle tracking analysis

Undiluted pre-cleaned CSF samples were analyzed by NTA according to manufacturer's instructions using a NanoSight NS300 system (Malvern Technologies, Malvern, UK) configured with 532 nm laser. Ideal measurement concentrations were found by pre-testing the ideal particle per frame value (20–100 particles/frame). Following settings were set according to the manufacturer's software manual. A syringe pump with constant flow injection was used and three videos of 60 s were captured and analyzed with NTA software version 3.4. From each video, the mean, mode, and median EV size was used to calculate samples concentration expressed in nanoparticles/ml.

2.10. Peptide microarrays

Microarrays were arrayed with MSP on MCP-6 (Lucidant Polymers, Sunnyvail, CA) coated patterned silicon chips, with 80 nm oxide layer thickness, using a non-contact S12 Spotter (Scienion Co., Berlin, Germany), depositing 1 drop for each spot according to (Gori et al., 2020). Fifty μl of undiluted CSF samples were incubated for 2 h in static conditions on the printed chips in a humid chamber. After incubation, chips were moved on 24-wells plate, twice washes were performed for 2 min at 300 rpm on orbital shaker with filtered PBS. For fluorescence immune-staining, chips were incubated with a mix of antibodies anti-Tetraspannin (CD9, CD63 and CD8, Ancell, Bayport, MN, USA), anti-CD171 (neural cell adhesion molecule L1) or anti-TMEM119 (Transmembran protein 119), labelled with CF555® and CF647® (Biotium, San Francisco Bay Area, California, USA). Antibody specifications are reported in Table 2. Each antibody was diluted 1:1000 in filtered incubation buffer (Tris/HCl pH 7.6 0.05 M, NaCl 0.15 M, Tween20 0.02%), and chips were incubated dynamically at 300 rpm for 15 min. The chips were then washed in filtered PBS twice time followed by a rinse and dry in MilliQ water. The chips were then imaged with the ExoView R100 reader using the nScan 2.8.4 acquisition software. The data were analyzed using ExoView Analyzer.

2.11. Western blot analysis

EV samples were mixed with a modified version of Laemmli buffer (2% SDS, 20 mM Tris pH 6.8, 2 mM EDTA, 10% glycerol, 2% β-mercaptoethanol, 0.01% bromo-phenol blue) at a final 1× concentration and loaded on a 12% SDS polyacrylamide gel. Proteins were separated by gel electrophoresis, blotted on a 0.2 μm nitrocellulose membrane (GE HealthCare Amersham), and probed overnight at 4 °C using the primary antibodies reported in Table 2. After washing, membranes were incubated with the horseradish peroxidase-conjugated secondary antibodies (Pierce, Thermo Fisher Scientific, Waltham, MA, USA) for 1 h and immune-positive bands were detected by chemiluminescence (ECL, Euroclone, Milan, Italy, WESTAR-ONE Plus, Cyanagen, Bologna, Italy, or FEMTO ThermoFisher, Waltham, MA, USA) according to the manufacturer's instructions.

Table 2
Antibody specifications.

Antibody	Supplier	Identifier	Dilution
Mouse anti-Actin	Merck	Cat# A4700	1:4000
Mouse anti-ALDH1L1	Sigma-Aldrich	Cat# MABN495	1:500
Rabbit anti-Annexin-2	Abcam	Cat# ab41803	1:500; 1:5000
Rabbit anti-Calnexin	Sigma-Aldrich	Cat# C4731	1:1000
Mouse anti-CD171	Thermo Fisher Scientific	Cat# 14–1719-82	1:1000
Mouse anti-CD68	Bio-Rad	Cat# MCA5709	1:500
Mouse anti-CNPase	Millipore	Cat# MAB326	1:500
Mouse anti-Flotillin-1	BD Biosciences	Cat# 610820	1:1000
Rabbit anti-GAPDH	Synaptic Systems	Cat# 247002	1:5000
Mouse anti-GFAP	Merck	Cat# G3893	1:1000
Rabbit anti-GM130	Gently provided by Rr. Renz	Ref. (Seelig et al., 1994)	1:1000
Rabbit anti-GPR17	Homemade	Ref. (Ciana et al., 2006)	2 μg/mL
Rabbit anti-GST-π	VODEN	Cat# 312	1:500
Rabbit anti-hSOD1	Enzo Life Sciences	Cat# ADI-SOD-100-D	1:1000
Rabbit anti-IBA1	Wako	Cat# 016–20,001	1:1000
Mouse anti-MAP2	Immunological science	Cat# MAB-10784	1:1000
Rabbit anti-OLIG2	Sigma-Aldrich	Cat# AV32752	1:1000
Rabbit anti-PLP1	Sigma-Aldrich	Cat# SAB2101830	1:500
Rabbit anti-PTX3	Thermo Fisher Scientific	Cat# PA5–98102	1:500
Rabbit anti-SP1	Sigma-Aldrich	Cat# 07–645	1:500
Mouse anti-TMEM119	Biolegend	Cat# 853302	1:1000
Rabbit anti-TOM20	Santa Cruz Biotechnology	Cat# sc-11,415	1:500
Mouse anti-Tubulin β3	Biolegend	Cat# MMS-435P	1:5000

Total protein concentration of spinal cord homogenates was assessed through Pierce™ BCA Protein Assay Kit (Thermo Fisher Scientific, Waltham, MA, USA). Five-forty μg of each tissue homogenate, added with Laemmli sample buffer, were separated by SDS-PAGE gel electrophoresis using the appropriate concentration of acrylamide (7–15%), and electrophoretically transferred to 0.2 or 0.45 μm nitrocellulose membranes (GE HealthCare Amersham). Membranes were blocked overnight in 4% non-fat milk (Hipp 2) in Tris-buffered saline (TBS) at 4 °C, incubated for 2 h with the primary antibodies and then with the suitable horseradish peroxidase-conjugated secondary antibodies. After washing with TBS and decreasing concentrations of Tween® 20 (starting from 0.3% to 0%), immune-positive bands were detected with chemiluminescent reagent Clarity or Clarity Max (Bio-Rad, Hercules, CA, USA). Primary antibodies specifications and used concentrations are listed in Table 2.

Immunoreactive bands were quantified by ImageJ software (http://imagej.nih.gov/ij/). Values from the Tg samples were normalized to the age-matched control always run on the same SDS-PAgel. Each Tg/Wt sample pair was run 3 times and mean values of the triplicate results for each animal were used as individual data for statistical analysis. For spinal cord analysis, values have been normalized over a suitable housekeeping protein (GAPDH or β-actin).

2.12. Statistical analyses

Sample sizes for all experiments were based on availability of swine tissues and biological fluids and are provided in the figure legends. Statistical analysis was performed using GraphPad Prism 8 software (San Diego, CA, USA). All data sets were tested for normal distribution using Kolmogorov–Smirnov tests and the analysis of outliers, and the appropriate statistical test was then selected accordingly. The statistical analysis of AChR-γ and NFL data of Tg animals at different disease stages respect to Wt pigs was made using Kruskall-Wallis test followed by Dunn's multiple comparison test, given the small sample sizes in late-asymptomatic and symptomatic groups. For WB analysis, each Tg animal was normalized over to the corresponding age-matched Wt animal and unpaired Student's *t*-test or Mann-Whitney was used to compare the differences in protein expression. Differences were considered significant when $p < 0.05$ and indicated by asterisks: $*p < 0.05$, $**p < 0.01$, $***p < 0.001$. If not otherwise specified, data are shown as means ± SEM.

3. Results

3.1. Clinical, neurological and pathological examination

A group of 16 hSOD1^{G93A} Tg pigs was investigated before overt clinical symptoms, at an early (7 animals) and late (4 animals) asymptomatic stages, and after the onset of clinical symptoms at a symptomatic stage (5 animals). Pre-symptomatic animals were mostly females while symptomatic pigs were only males, due to the limited availability of Tg animals (Table 1A). Age-matched Wt animals, both male and female, were used as controls (Table 1B). Disease onset and survival time of Tg pigs were evaluated using Kaplan-Meier survival estimates and log-rank tests (Fig. 1A). Average age of onset was 38.8 months (±3.55) and mean survival time was 39.18 months (±3.56). The average time between the onset of symptoms and the death or sacrifice of the animals was 11.4 days, revealing that at the time of symptom onset animals were already in a terminal phase of the disease and typically reached the endpoint in a short time. During disease manifestations, as already

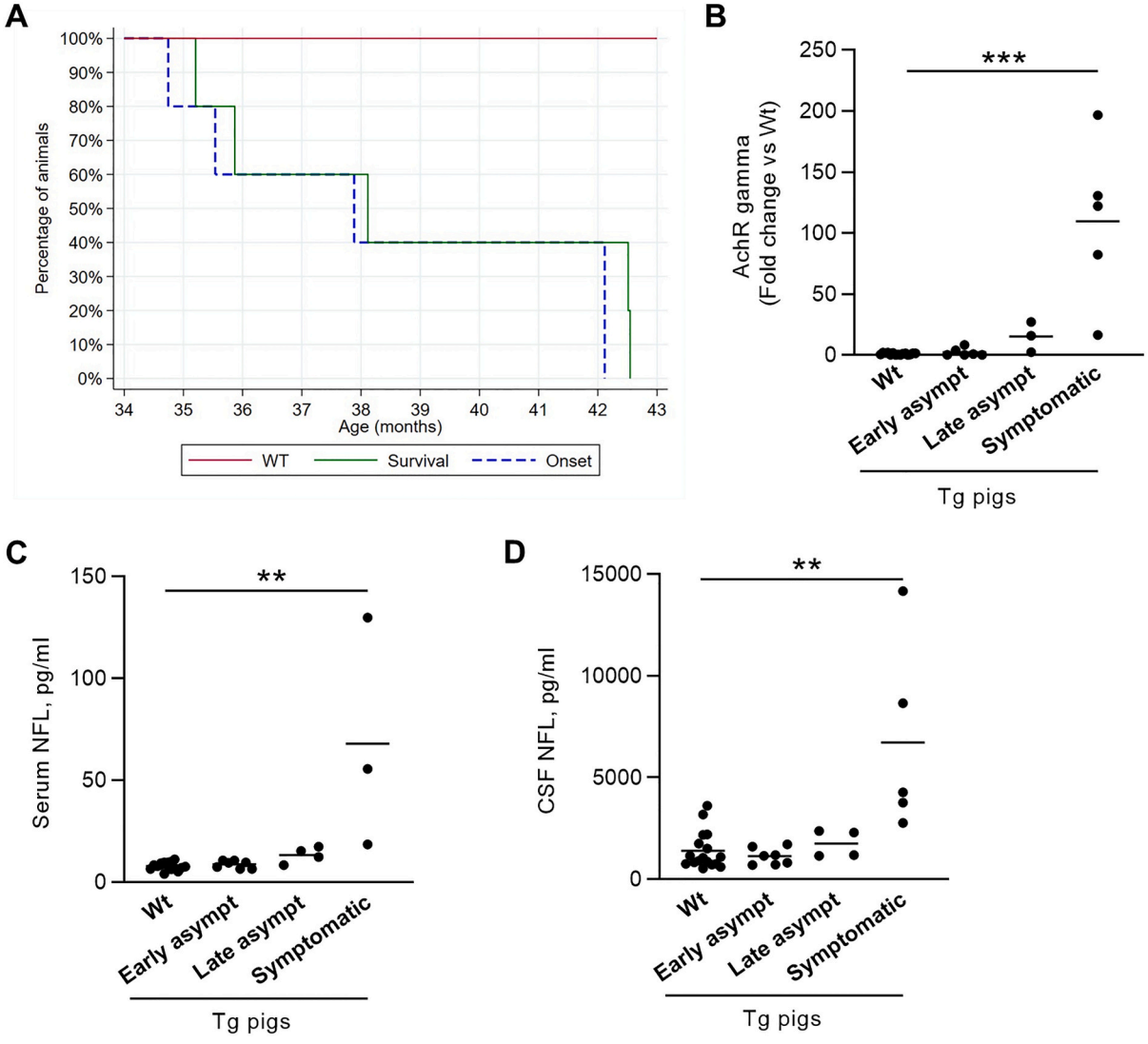

Fig. 1. Clinical and neuropathological features of hSOD1^{G93A} Tg pigs. **A**) Kaplan Meier curves showing disease onset and survival time of Tg pigs. **B**) Expression of the nicotinic acetylcholine receptor fetal subunit gamma (AchRγ) mRNA in the diaphragm of Tg pigs at early asymptomatic ($n = 6$), late asymptomatic ($n = 3$) and symptomatic ($n = 5$) stages compared to age-matched Wt. Data are expressed as fold changes with respect to the mean of Wt of the same age range. For graphical simplicity, the Wt were merged as there were no significant differences between the pigs at different ages. Statistical analysis was made on the individual 2-ΔCt. **C**—**D**) NFL concentration in serum **(C)** and CSF **(D)** of Tg pigs at early asymptomatic ($n = 7$), late asymptomatic ($n = 4$), and symptomatic ($n = 3$ for serum and $n = 5$ for CSF) stages compared to age-matched Wt ($n = 16$). Data are expressed as pg/mL. Each dot represents mean values of the triplicate results for each animal. Kruskall Wallis test followed by Dunn's multiple comparison test, $**p < 0.01$, $***p < 0.001$ Tg animals grouped according to their clinical signs *vs* Wt pigs.

reported by Crociara and colleagues (Crociara et al., 2019), animals mainly showed respiratory distress, gait abnormalities and sometimes dysphagia. Gait alterations consisted in progressive ataxia and hypermetria, worsening to sternal and subsequently lateral recumbency. Mental status became progressively obtunded with worsening of the clinical picture. The characteristics of hSOD1^{G93A} Tg pigs are reported in Table 1. Since labored breathing occurred in concomitance with motor deficit and, in some pigs, acute respiratory failure even preceded the motor impairment leading to sudden death, we examined the expression level of AChR gamma subunit transcript in the diaphragm as a marker of muscle denervation. Indeed, the nicotinic AChR in adult skeletal muscle endplate forms a heteropentamer consisting of α1β1δ subunits with one ε-subunit that is replaced by a fetal γ-subunit following muscle denervation (Goldman et al., 1988). A progressive increase in γ-subunit AChR transcript levels was observed at the late asymptomatic and symptomatic stages, although with high variability between pigs (Fig. 1B). We also measured the serum and CSF concentrations of NFL, a sensitive biomarker of neuroaxonal degeneration, in Tg pigs at the different stages of the disease in comparison with age-matched Wt pigs. A significant increase of NFL was found only at a symptomatic stage in both plasma and CSF(Fig. 1C and D). These results suggest that diaphragm denervation precedes the symptomatology of these pigs and justify the biochemical analyses carried out at the level of the cervical spinal cord which is where the motor neurons of the phrenic nerve originate for the innervation of the diaphragm.

3.2. Biochemical changes in the spinal cord of Tg pigs during disease development

Previous work showed that hSOD1^{G93A} Tg pigs share several neuropathological features of ALS, including motor neuron atrophy, microgliosis, astrogliosis, myelin alterations and muscle pathology (Chieppa et al., 2014; Crociara et al., 2019) at end-stage of the disease. From the progenitor, described in Crociara and colleagues (Crociara et al., 2019), many other hemizygous Tg animals have been created and sacrificed at early and late asymptomatic stages and at end-stage symptomatic phase (6, 4 and 5 animals, respectively), allowing to investigate whether biochemical changes may precede disease onset. To this aim, we first analyzed by WB the spinal cord cervical tracts of 15 Tg pigs, stratified according to their clinal signs, and age-matched Wt animals with antibodies specific for human SOD1 (hSOD1) to check the expression levels of mutant hSOD1 in Tg pigs during disease progression. Analysis showed that Tg pigs express the hSOD1 approximately at the same level at asymptomatic and symptomatic stages (Fig. 2A). The anti-hSOD1 antibody used to detect the transgenic protein also detected a band of approximately 20 kDa, both in Wt and Tg animals, that corresponds to the endogenous swine SOD1 (swSOD1) (Fig. 2A).

Next, we compared the expression of key glial markers in the spinal cord of Tg and age-matched Wt pigs. Immunoblot for Aldehyde dehydrogenase 1 family member L1 (ALDH1L1), a pan astrocytic marker, revealed an increased protein levels in Tg pigs, either pooled together (Fig. 2B) or grouped according to their clinical signs in early asymptomatic, late asymptomatic, and symptomatic animals (Fig. 2C). Specifically, ALDH1L1 content was already higher, >3 times, in late asymptomatic Tg pigs compared to the corresponding Wt animals and remained significantly elevated in symptomatic pigs (Fig. 2C). Similar changes were observed in the content of Pentraxin 3 (PTX3), a reactive astrocyte marker, which was significantly increased in late asymptomatic and symptomatic pigs compared to Wt animals (by 2.3-fold and 4.7-fold, respectively; Fig. 2B and C). Of note, both astrocytic markers were more abundant in Tg animals showing motor deficits (pigs #20 and #23; Fig. 2C, red dots) compared to Tg pigs without motor symptoms (pigs #21, #26 and #27; Fig. 2C, green dots).

Analysis for the microglial marker TMEM119, a homeostatic gene downregulated in disease-associated microglia (Keren-Shaul et al., 2017), revealed no changes in Tg pigs, either pooled together or grouped according to their clinical signs, compared to the corresponding Wt animals (Fig. 2D and E). However, small reductions in TMEM119 levels could be masked by an increased microglial density in the spinal cord of Tg pigs, as previously reported (Crociara et al., 2019). Consistent with microglia activation, we found higher levels of CD68, a lysosomal microglial protein indicative of augmented phagocytosis, in Tg pigs compared to Wt animals (by 1.8-fold; Fig. 2D), especially at symptomatic stage in pigs with motor symptoms (pigs #20 and #23; Fig. 2E, red dots).

Immunoblotting for the pan oligodendrocyte marker OLIG2 revealed a strong upregulation (by 4.5-fold) in Tg pigs (Fig. 2F), already significant at early asymptomatic stages and further augmented at late asymptomatic and symptomatic stages (Fig. 2G). The G protein-coupled receptor 17 (GPR17), which is abnormally increased in oligodendrocytes under disease conditions characterized by myelin defects (Bonfanti et al., 2020), showed a trend to upregulation in symptomatic Tg pigs (Fig. 2G), while Glutathione-S-transferase-pi (GST-π), a marker of both oligodendrocyte progenitor cells (OPCs) and mature oligodendrocytes (Tamura et al., 2007), was significantly higher (by 5-fold) in Tg pigs compared to Wt animals (Fig. 2F) showing a strong upregulation at late asymptomatic stages and in symptomatic animals with motor symptoms (Fig. 2G). No changes in the protein expression of proteolipid protein 1 (PLP1) and Cyclic nucleotide 3′-phosphodiesterase (CNPase), markers of differentiated oligodendrocytes, were observed in Tg pigs in the course of the disease (Fig. 2F-G). Taken together these findings suggest that progressive OLIG2 upregulation in Tg pigs could result from proliferation and/or recruitment of pre-oligodendrocytes in the spinal cord of Tg animals rather than increase in the density of fully differentiated oligodendrocytes.

Finally, the expression of the neuronal marker Tubulin β3 (Tub β3) did not reveal major changes in the cervical tract of spinal cord between Wt animals and Tg pigs, either pooled together (Fig. 2H) or grouped according to their clinical signs in early asymptomatic, late asymptomatic, and symptomatic animals (Fig. 2I).

In conclusion, our analyses revealed an increase of some astrocytic, microglial and oligodendrocytic markers in the cervical track of the spinal cord of hSOD1^{G93A} Tg pigs, suggesting a stressful response of astrocytes, microglia, and immature oligodendrocytes to the mutant SOD1. Interestingly, astrocytes- and oligodendrocytes-lineage markers were increased before the appearance of the symptoms. Importantly, animals showing motor deficits displayed larger alterations in the marker expression compared to animals without motor symptoms.

3.3. hSOD1^{G93A} pigs don't show major alterations in EV release

CSF samples collected from hSOD1^{G93A} and Wt pigs were precleaned from cells and debris, inspected for red blood cell contamination and used for direct measurements of nanoparticles (presumed as *EVs*) (Fig. 3A). TPRS analysis on all Tg pigs and Wt animals, showed that nanoparticles were highly heterogeneous in size in both Tg and Wt pigs, ranging from 80 nm to 560 nm but had similar mode values of size distributions and mean diameter (Fig. 3B). No changes in nanoparticle concentrations were observed between Wt and Tg pigs (Fig. 3C). NTA analysis confirmed that CSF nanoparticles from all hSOD1^{G93A} Tg pigs and Wt animals had similar mode values and mean diameter (Fig. 3D), as well as particle concentration (Fig. 3E).

3.4. EV production from brain cells increases at late asymptomatic stage in hSOD1^{G93A} pigs

Purity of CSF EVs was assessed by WB analysis for positive and negative EV markers using spinal cord homogenates as positive control for non-EV markers. The analysis was performed on a mixed population of EVs (small and large EVs) ultracentrifugated at 100,000 x g from 3 ml of pre-cleared CSF collected from a hSOD1^{G93A} Tg pig and an age-matched Wt animal (Fig. 3A). EVs from both Wt and Tg pigs were

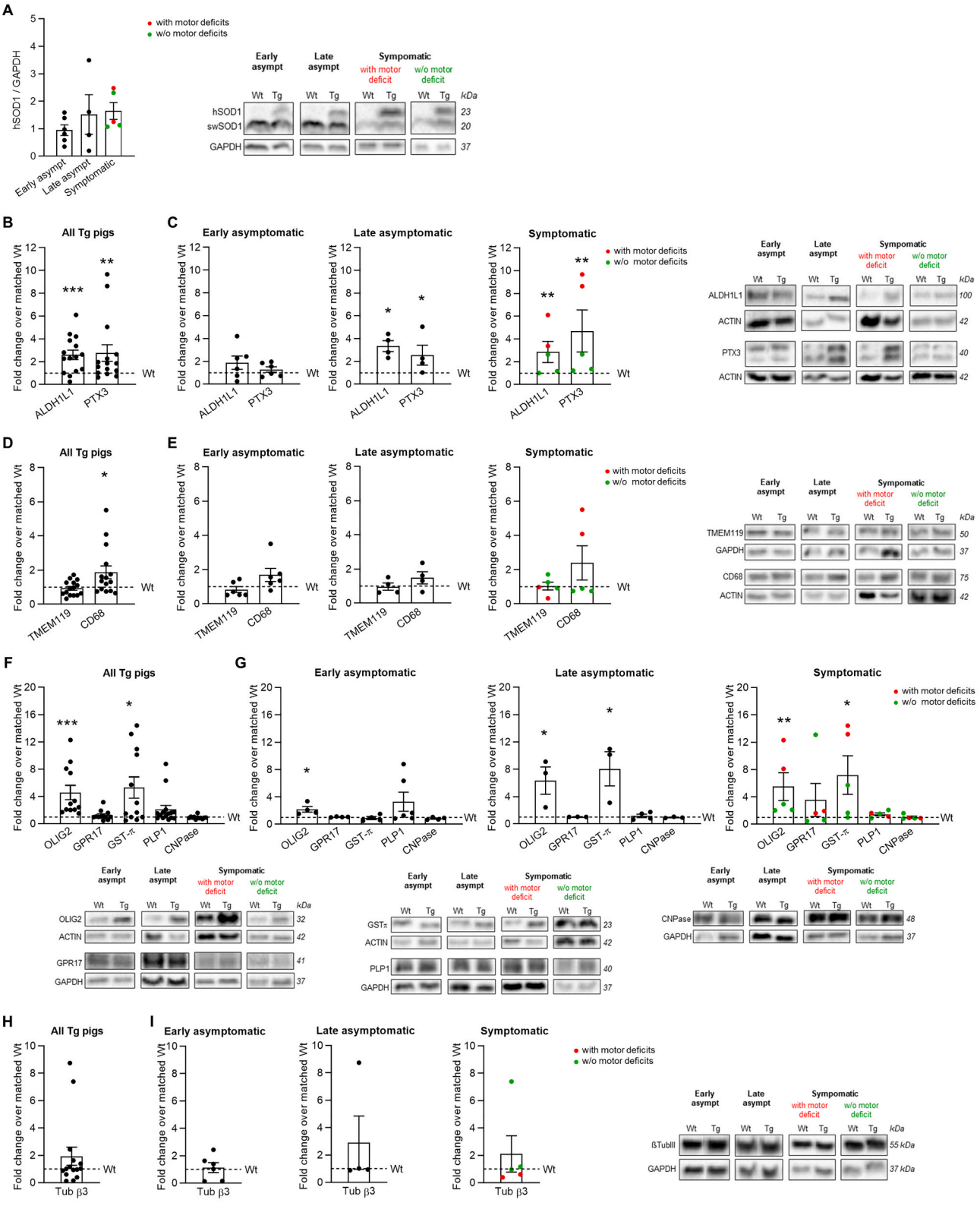

Fig. 2. Expression of glial and neuronal markers in cervical spinal cord of hSOD1^{G93A} Tg pigs. **A)** Representative Western blot and relative expression of the transgenic human SOD1 (hSOD1) in Tg pigs grouped according to their clinical signs. **B—I)** Representative Western blot and relative expression of astrocytic markers ALDH1L1 and PTX3 **(B—C)**, microglial markers TMEM119 and CD68 **(D-E)**, oligodendrocyte markers OLIG2, GRP17, GST-π, PLP1 and CNPase **(F-G)** and neuronal marker Tubulin β3 **(H—I)** in Tg pigs grouped altogether or according to their clinical signs. Cell lineage marker expression is normalized over housekeeping proteins GAPDH or actin, as indicated in representative images, and over age-matched Wt animals. Wt, $n = 15$ pigs; Tg, n = 15 pigs. All samples were analyzed in two or three independent experiments for each marker and each dot represents mean values of the replicate results for each animal. Red and green dots indicate symptomatic animals with and without motor deficits, respectively. Student's *t*-test or Mann-Whitney test, $^{*}p < 0.05$, $^{**}p < 0.01$, $^{***}p < 0.001$ marker expression in Tg animals *vs* Wt animals (dashed lines). (For interpretation of the references to colour in this figure legend, the reader is referred to the web version of this article.)

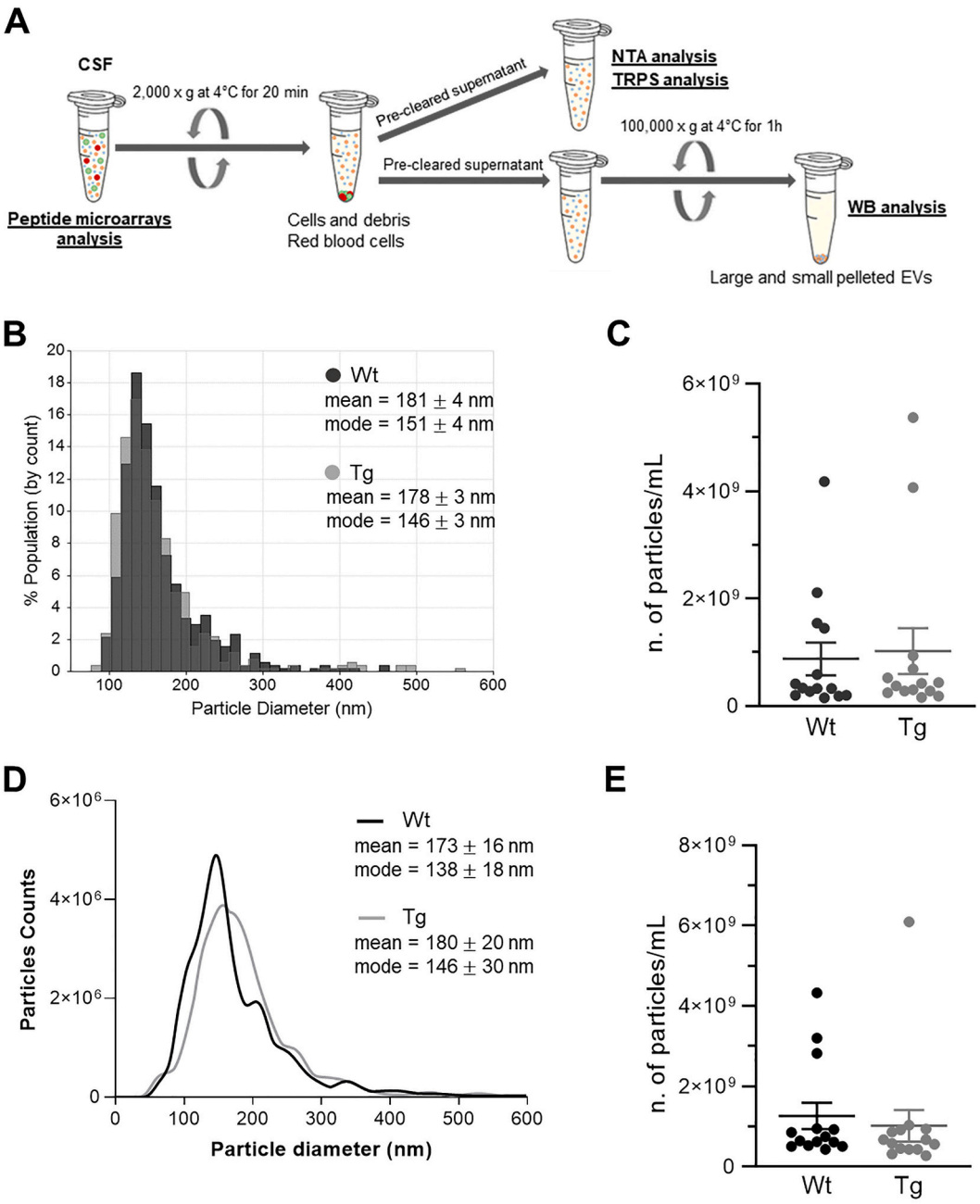

Fig. 3. EV size and concentration measurements in CSF of hSOD^{G93A}Tg animals. **A)** Schematic representation of CSF EVs isolation based on differential centrifugation. **B)** Representative size distribution of CSF EVs from Tg and Wt pigs detected by TRPS. **C)** Scatter dot plot showing the number per mL of EVs derived from CSF of Tg and Wt pigs analyzed by TRPS. **D**) Size profile of EVs from Tg and Wt pigs detected by NTA. **E**) Scatter dot plots showing the number per mL of EVs derived from CSF of Tg and Wt pigs analyzed by NTA. Wt, $n = 14$ pigs; Tg, n = 14 pigs. Dots represent mean values of measurement replicates for each animal.

positive for the EV markers Flotillin1 and Annexin-A2 (AnnxA2) and negative for intracellular organelle markers (GM130, TOM20, Calnexin and SP1 for Golgi, mitochondria, endoplasmic reticulum, nuclei, respectively) or the cytosolic marker GAPDH (Fig. 4A). The markers of contamination were evident only in the spinal cord homogenates (Fig. 4A).

Next, we asked whether the concentration of EVs generated by different brain cell subpopulations might be altered in the CSF of hSOD1^{G93A} Tg pigs compared to age-matched Wt animals, reflecting a change in the activation state and/or a stressful response of the cells to mutant SOD1. We tested several brain cell lineage markers on swine EVs and found immunoreactivity for the astrocyte markers ALDH1L1 and Glial Fibrillary Acidic Protein (GFAP), the neuronal markers CD171 and Microtubule-Associated Protein 2 (MAP2), the microglia marker TMEM119, the myeloid marker IBA1, and the oligodendrocyte marker PLP1 (Fig. 4B). Four lineage markers, *i.e.* CD171, ALDH1L1, TMEM119 and PLP1, were then selected for analysis of EV samples extracted from CSF (2 ml) of all Tg and Wt animals. We found that EVs in the CSF of Tg pigs were more immunoreactive for TMEM119 (by 2.7-fold) compared to Wt EVs (Fig. 4C). Given that the TMEM119 is downregulated upon microglia activation, higher TMEM119 immunoreactivity reflected higher production of microglial EVs or larger microglia population in hSOD1^{G93A} Tg pigs, rather that TMEM119 upregulation in Tg EVs. When Tg pigs were grouped by disease stages higher microglial EV production was detected at all phases, but differences were no longer statistically significant (Fig. 4D). Conversely, higher immunoreactivity for the

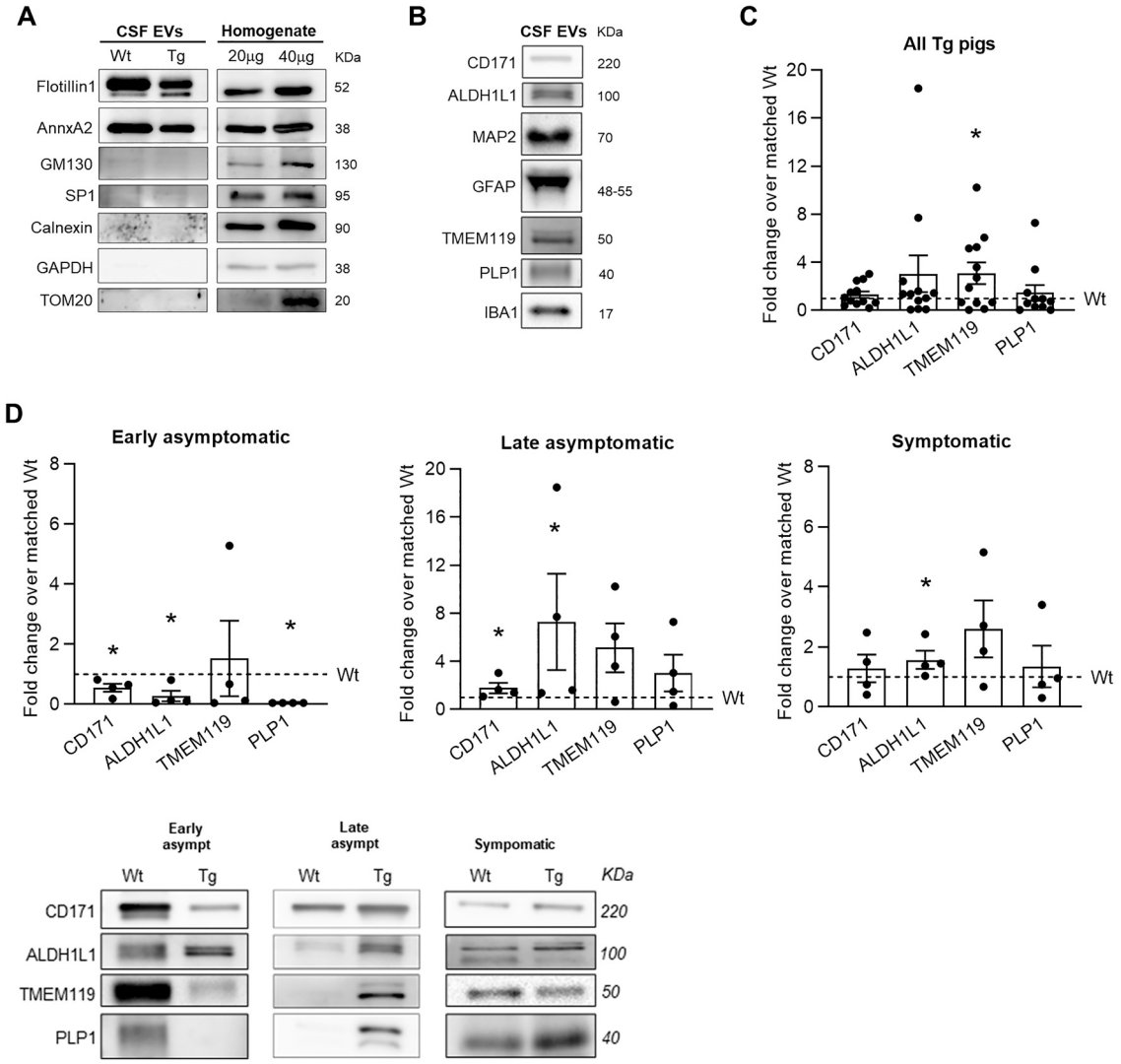

Fig. 4. Comparative analysis of EVs positive for brain cell lineage markers in the CSF of Tg and Wt pigs. A) Western blot analysis for EV positive markers Flotillin1 and Annexin-A2 (AnnxA2), and negative markers GM130, TOM20, Calnexin, SP1 and GAPDH in spinal cord homogenates (20 μg and 40 μg) and EVs pelleted from 3 mL of CSF. B) Representative Western blot of brain cell lineage markers in EVs pelleted from 2 mL of CSF. C—D) Representative Western blot and relative expression of CD171, ALDH1L1, TMEM119 and PLP1 in EVs derived from CSF (2 mL) of Tg pigs grouped altogether (C) or according to their clinical signs (D), normalized to the corresponding age-matched Wt animals. Wt, $n = 12$ pigs; Tg, n = 12 pigs (4 early asymptomatic, 4 late asymptomatic, and 4 symptomatic). Dots represent means values of measurement replicates for each animal. Student's *t*-test or Mann-Whitney test, $*p < 0.05$ marker expression in Tg animals *vs* Wt animals (dashed line).

neuronal marker CD171 (by 1.6-fold) and the astrocytic marker ALDH1L1 (by 7.3-fold) was observed at late asymptomatic stage in Tg EVs compared to Wt animals (Fig. 4D), suggesting higher EV release from both neurons and astrocytes. After the onset of symptoms, EV production from neurons went back to Wt levels while EV release from astrocytes remained higher (by 1.4-fold) in Tg pigs (Fig. 4C). These data suggest that the activation of neurons, astrocytes, and microglia precedes the onset of disease symptoms, and point to a sustained activation of astrocytes and microglia in this ALS model.

3.5. Membrane sensing peptide enabled on-chip analysis for EV co-localization of TMEM119 or CD171

We next sought to develop a purification-free method enabling direct measurements of specific EV subpopulations in the CSF, providing fast results with a low consumption of sample volume. Generally, NanoView platform makes use of antibody microarrays where EVs are captured by anti-tetraspanins (CD9 or CD63 or CD81), which are considered quite general EV surface markers. Using the ExoView Tetraspanin Kit we have recently demonstrated a limit of detection for EVs isolated by cell culture in the range of 10^7–10^8 EV/ml depending on targeted tetraspanins (Frigerio et al., 2022). The low concentration of EVs (10^8 particle/ml) in CSF is close to the limit of detection of this kit, making it difficult, if not impossible, to reliably detect sub-populations of CSF EVs without introducing an enrichment step. To overcome this limitation, we took advantage of a recently developed approach for universal EV capturing based on the use of a bradykinin-derived Membrane Sensing peptide (MSP) (Gori et al., 2020), which captures small EVs based on specific yet general membrane traits such as charge, lipid defects and curvature. The MSP exhibits a capturing capacity much higher than antibodies and the on-chip binding is independent by differential expression of tetraspanins (typically used for capture), thus representing an unbiased platform for subsequent immune-staining with antibodies for putative biomarkers discovery/validation.

Microarrays spotted with MSPs were used to analyze CSF from $hSOD1^{G93A}$ and Wt pigs; the small EVs were captured by the peptide spots and incubated with a mixture of anti-CD9/CD63/CD81 labelled with CF555® fluorescent antibodies to confirm the EV nature of

captured particles and either with anti-CD171 or anti-TMEM119 antibody labelled with CF647® (Fig. 5A). Thus, the analyses co-localize the specific surface markers on captured EVs and provides a count of the neuron and microglia-derived EV subpopulations, respectively. Fifty μL of CSF of Tg pigs at symptomatic stage and age-matched Wt pigs were analyzed without any prior treatment except for a short pre-clearing step (2000 x g for 20 min). We considered the co-localization data only, that is the particles that are simultaneously positive for the two fluorescence channels: tetraspanin CD9/CD63/CD81 and one of the biomarkers under investigation (CD171 or TMEM119). All co-localization data used to compare Tg and Wt pigs were normalized for the total number of positive tetraspanin particles.

Results of co-localization (double tetraspanin and CD171 positive) showed no changes in the content of neuron-derived EVs in the CSF of Tg symptomatic pigs with respect to Wt animals, confirming WB measurements (Fig. 5B). In addition, the analysis revealed a significant increase in the concentration of microglia-derived EVs in the CSF of Tg pigs compared to Wt animal (double tetraspanin and TMEM119 positive), in line with the trend to increased production detected by WB (Fig. 5B).

3.6. Brain cell-derived EVs in plasma do not reflect the concentration changes observed in the CSF of Tg pigs

We next investigated whether altered concentration of brain cell-derived EVs in the CSF of Tg pigs might also be detected in the plasma. By WB analysis, we compared immunoreactivity for neuronal and glial specific markers in EVs isolated by the commercial kit EXOQ from an equal volume of plasma (250 μl) from hSOD1^{G93A} pigs and Wt animals. We didn't find significant differences in plasma EV immunoreactivity for CD171, ALDH1L1, TMEM119 and PLP1 in all Tg pigs *versus* age-matched Wt (Fig. 6A). Only at symptomatic stage ALDH1L1 and TMEM119 immunoreactivity showed a trend to increase and PLP1 staining increased significantly (by 2-fold) in plasma EVs from Tg pigs relative to Wt pigs (Fig. 6B). These data indicate that alterations in the amount of brain cell-derived EVs in plasma, do not mirror the changes that arise already at a late symptomatic stage in CSF.

4. Discussion

Tg pigs expressing hSOD1^{G93A} are characterized by a long asymptomatic phase that precedes ALS symptoms and neuropathological alterations, offering a unique opportunity to investigate early mechanisms affected in the disease. However, whether and at which disease stage neural cell alterations occur in hSOD1^{G93A} pigs is completely unexplored.

In this study we monitored by WB the expression of neuronal and glial cell markers in the cervical tract of spinal cords of hSOD1^{G93A} Tg pigs at early and late asymptomatic stages, before overt clinical symptoms, and at the symptomatic stage in comparison to age-matched Wt animals. In addition, we evaluated by WB the amount of EVs of neuronal and glial origin in the CSF and plasma during the disease course, as EV production normally increases in response to stressful/pathological conditions (Verderio et al., 2012; Agosta et al., 2014; Yin et al., 2021). For EVs derived from neurons and microglia, the quantification was corroborated by an *ad hoc* purification-free method that enables fast EV measurements in a low sample volume of biological fluid.

We show that oligodendrocytes are the first brain cells activated in spinal cord cervical tracts of hSOD1^{G93A} pigs at early asymptomatic stage, followed by astrocytes at late asymptomatic stage, releasing more EVs in the CSF at this disease stage. Microglial cells were also altered in spinal cord of Tg pigs and showed a trend to increased EV production at both asymptomatic and symptomatic stages. Interestingly, these changes occur earlier than the raise of NFL, an established marker of neurodegeneration, indicating that EV production is an early mechanism affected in the ALS CNS tissue. We show no correlation between the content of EVs of neuronal and glial cell origin in CSF and plasma, questioning that the amount of plasma EVs positive for central nervous system (CNS) lineage markers may mirror the activation state of brain resident cells.

4.1. Oligodendrocytes are the first cells altered in the hSOD1^{G93A} Tg CNS tissue

A key finding of this study is the demonstration of a very early activation of Olig2 positive cells in the spinal cord of Tg pigs, that comes several months before the onset of clinical symptoms and further increases at late asymptomatic stages. Olig2 upregulation likely reflects proliferation of OPCs rather than increased density of myelinating oligodendrocytes, whose phenotypic markers PLP1 and CNPase do not change during disease progression. The increased expression of GST-π, a marker of both OPCs and mature oligodendrocytes (Tamura et al., 2007) and tendency to upregulation of GPR17, a G protein-coupled receptor downregulated in myelinating oligodendrocytes (Fumagalli et al., 2011; Chen et al., 2009), at late asymptomatic and/or symptomatic stages, further suggests accumulation of OPCs/pre-oligodendrocytes in Tg pigs, which may be unable to differentiate to fully mature oligodendrocytes and support motor neuron survival. However, the absence of OPC specific antibodies, such as Neural/glial antigen 2 (NG2) or Platelet-Derived Growth Factor Receptor Alpha (PDGFR-α), working in the swine did not allow us to directly prove an increased pool of OPCs in the spinal cords of Tg pigs. Neither it made possible to explore possible changes in EV

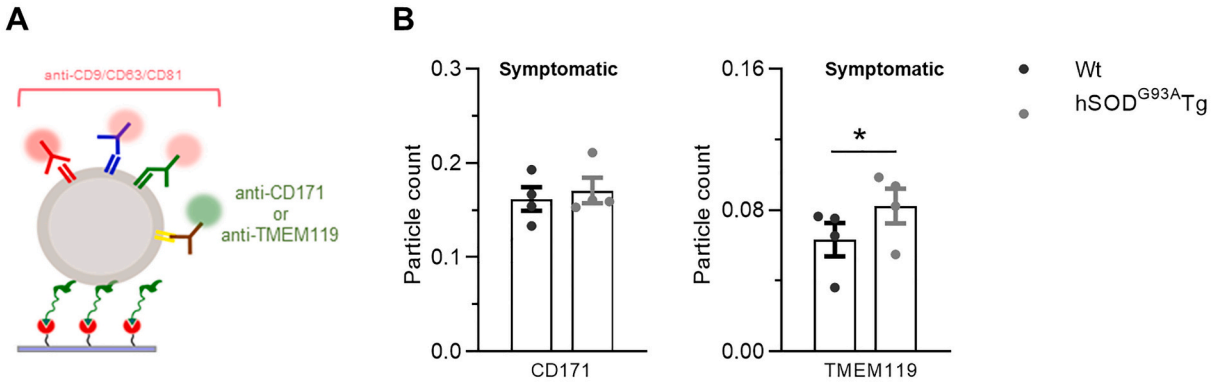

Fig. 5. Evaluation of neuron- and microglia-derived EV production in CSF of Tg animals by ExoView platform. **A)** Scheme of assay: MSP was used as capture on silicon chip and EV phenotyping was performed by fluorescence Anti-tetraspanins and Anti-TMEM119 or Anti-CD171 antibodies. B) Co-localized data were used to compare CD171- or TMEM119- positive EVs in Wt and symptomatic Tg animals. Wt, $n = 4$ pigs; Tg, n = 4 pigs. Dots represent means values of measurement replicates for each animal. Student's *t*-test, $^*p < 0.05$.

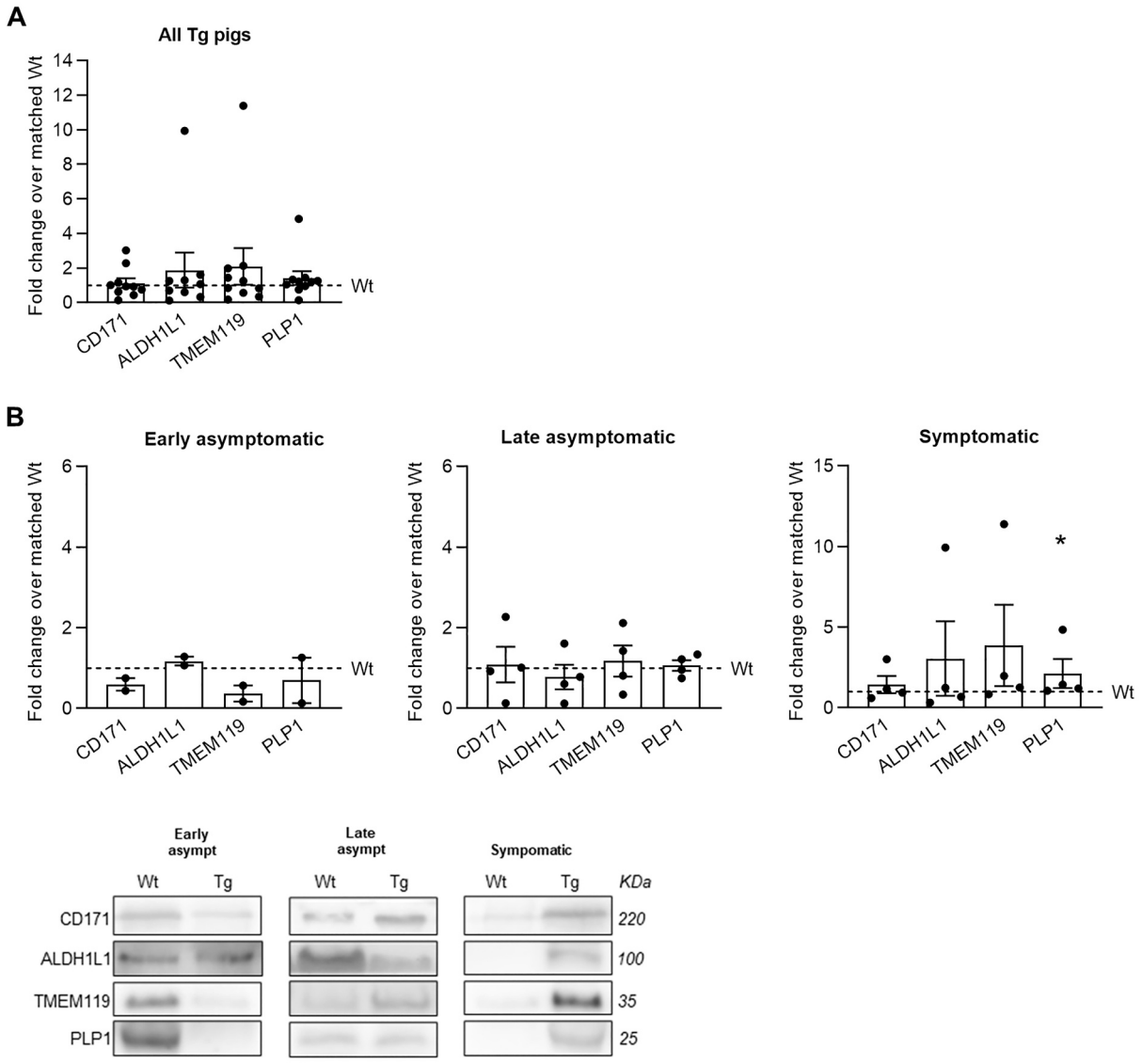

Fig. 6. Comparative evaluation of EVs positive for brain cell lineage markers in the plasma of Tg and Wt pigs. A-B) Representative Western blot and relative expression of CD171, ALDH1L1, TMEM119 and PLP1 in EVs derived from plasma of Tg pigs grouped altogether (A) or according to their clinical signs (B), normalized to the corresponding age-matched Wt animal animals. Wt, $n = 10$ pigs; Tg, n = 10 pigs (2 early asymptomatic, 4 late asymptomatic, and 4 symptomatic). Dots represent means values of measurement replicates for each animal. Student's t-test or Mann-Whitney test, $^{*}p < 0.05$ marker expression in Tg animals *vs* Wt animals (dashed line).

production from OPCs at asymptomatic disease stages, a hypothesis that is worth to be verified in both Tg pigs and human ALS patients. In agreement with our data, previous studies showed i) enhanced proliferation of NG2 positive OPCs prior to motor neuron degeneration in the spinal cord of $SOD1^{G93A}$ ALS mice (Kang et al., 2013; Philips et al., 2013), which may be interpreted as a compensatory response to promote regeneration of myelin forming cells (Bonfanti et al., 2020) and ii) depletion in myelin-oligodendrocyte glycoprotein (MOG) in EVs extracted from the extracellular space of the Tg ALS mouse brains (Silverman et al., 2019), which is indicative of myelination dysfunction.

4.2. EV release in the CSF reflects astrocytes and microglia activation in the spinal cord of Tg pigs

Astrogliosis and microgliosis are universal features of ALS, and the intensity of astrocyte and microglia activation has been correlated with severity of motor neuron damage in the human disease (Lasiene and Yamanaka, 2011). This trend is supported by the present study as we found gliosis and a progressive diaphragm denervation as result of motor neuron degeneration in the cervical tracts of spinal cord.

The main accomplishment of our study is the establishment of a link between astrocyte and microglia activation in the spinal cord and the content of EVs of astrocytic and microglial origin in the CSF of Tg pigs. This association is indicated by simultaneous evaluation of glial cell marker expression in the spinal cords and EVs isolated from the CSF of Tg pigs. The quantification of glial EVs in the CSF have been previously shown to reflect the pathological response of glial cells to the diseased CNS, a tissue not easily accessible to direct examination (Colombo et al., 2012). However, simultaneous analyses of glial cell responses in the CNS tissue and quantification of glia-derived EVs in body fluids have not yet been carried out to prove whether EV production actually reflects the extent of glial cell activation *in vivo*. Indeed, a limitation of EV quantification studies in CNS pathologies has been the inability to correlate EV concentration in body fluids to the state of donor cells in the pathological brain tissue. To the best of our knowledge, this is the first study showing that production of astrocytic EVs, identified by the pan marker

ALDH1L1, reflects ALDH1L1 upregulation in the spinal cords of Tg pigs at late asymptomatic and symptomatic stages and that production of microglial EVs, identified by TMEM119 marker, correlates with higher CD68 expression in the spinal cord. In future studies the use of additional cell lineage markers, including OPC specific markers, will advance our understanding on the temporal course of brain cell activation during ALS course and clarify to which extent EV production correlates with the response of specific brain cell types to the mutant ALS gene. This may lead to the identification of EV-associated early disease biomarkers in hSOD1^{G93A} pigs, to be explored in ALS patients. This is particularly important because at the moment the only established biomarkers for ALS are neurofilaments, that are unspecific, intrinsically linked to the final event of the pathological process and do not provide hints on the pathogenic mechanism (Zucchi et al., 2020).

4.3. Brain cell-derived EVs in plasma do not match those present in the CSF

There remains debate in the field whether plasma EVs immunoreactive for CNS cell lineage markers come exclusively from the brain and spinal cord. By comparing the relative amounts of EVs derived from various CNS cell types in the CSF and plasma of Wt and Tg pigs, we herein show no correlation between the EV content of any brain cell type in the two biofluids. Changes in the amount of EVs produced by neurons, astrocytes, microglia and oligodendrocytes become detectable in plasma only in the symptomatic stage of the disease, not mirroring the alterations detected in the CSF and in the spinal cord in the late asymptomatic phase. This indicates that the release of brain-derived EVs in the CSF is not represented in plasma. We don't think that EVs produced in the CNS cannot pass the BBB but that blood EVs positive for CNS markers do not derive exclusively from the CNS. Cells immunoreactive for brain lineage markers are indeed present in peripheral organs, such as the enteric nervous system, and EVs positive for brain markers produced in the periphery may cause dilution of brain cell-derived EVs in the blood.

4.4. Peptide microarrays analysis for microglia-derived and neuron-derived EVs

Due to the low concentration of EVs in CSF (10^8 particle/ml), assessing the cell origin of EVs by WB requires large volume of CSF, a very precious specimen that it is collected by a quite invasive procedure. Moreover, the methods used to isolate and analyze CSF EVs by WB are time consuming and do not provide the actual number of EVs in the body fluids, thus being not suitable for translational studies. Alternative approaches for measuring the concentration of brain-derived EV subtypes in body fluids rely on two-step methods consisting of total EV collection first (by size exclusion chromatography or precipitation), followed by extraction of EV subpopulations by affinity capture with antibodies/lectins against cell lineage markers (Fiandaca et al., 2015; Goetzl et al., 2016; Scaroni et al., 2022; Visconte et al., 2023). However, even with these two-step procedures the analysis of the actual number of EVs in the body fluids is challenging when performed by classical methodologies such as TRPS or NTA, which cannot distinguish EVs from possible contaminants generated during the isolation/elution procedure.

One of the goals of our study was to take advantage of our biochemical data showing changes in the content of various CSF EV subpopulations (*i.e.* neurons, astrocytes, microglia, and oligodendrocytes) in Tg pigs to develop a purification-free method enabling direct measurements of EV subtypes in the CSF and providing fast results with a low consumption of sample volume.

We employed microarray chips for SP-IRIS coupled to fluorescence immune-detection of neuron- and microglia-derived EVs, for which antibodies (CD171 and TMEM119) against EV surface makers were available and working in swine. We show that MSP microarrays analysis provides EV measurements consistent with WB quantification. The approach we here introduced has several advantages: i) MSP has a superior capturing capacity over antibodies for single EV surface markers thus enabling direct analysis of a small volume of CSF containing EVs without need for a pre-concentration step; ii) MSP binds EVs based on a general affinity for small EV membrane, thus avoiding the risk of bias due to unevenly distributed tetraspanins, the most used proxy for pan-specific capture; iii) the co-localization analysis increases robustness of data by detecting the double-positive only particles, where tetraspanins are co-expressed with the putative biomarker under analysis. In synthesis, the MSP microarray may pave the way toward novel diagnostic tools for early ALS diagnosis based on direct quantification of EVs produced by brain cells, including astrocytes and OPC, in a small volume of CSF.

4.5. Limitations of the study

There is a general sex bias in the analyses of the study, as we analyzed mostly Tg female pigs at presymptomatic stages and only males at the symptomatic stage, a limitation due to the small number of animals available for the study. In addition, although we characterized EVs by multiple approaches, including techniques at single vesicle resolution such as Exoview e TRPS, we did not perform TEM, one of the methods proposed by the International Society of Extracellular Vesicles for EV characterization (Théry et al., 2018).

5. Conclusions

This study provides evidence for augmented EV production from astrocytes in hSOD^{G93A} Tg pigs before the onset of disease symptoms, mirroring donor cells activation in the spinal cord tissue. It also suggests that EV measurements from OPCs, the cells first activated in the ALS spinal cord, may be exploited for the discovery of early disease biomarkers in amyotrophic lateral sclerosis.

Funding

This work was supported by Fondazione Regionale per la Ricerca Biomedica POR FESR 2014—2020 under INTERSLA project, ID 1157625 and by MARVEL project to M.Cr. (grant agreement No. 951768) which has received funding from the European Union's Horizon 2020 research and innovation program.

Author contributions

Experimental concept and design: C.V., S.F.C., M.Cr., M.Ch., C.B. and V.B.; data collection and analysis: M.T.G., S.P., R.F., A.G., F.S., L.P. and C.M.; clinical examinations and sampling of animals: C.T., E.B., F.I., R. D., A.P., L.B., A.D.A., G.C.; writing—original draft preparation, C.V., M. T.G. and M.Cr.; writing—review and editing: S.F.C., R.F., C.G., A.P., S.P., C·C., E.B., C.B. and V.B.; supervision; C.V., S.F.C. and M.Cr.; funding acquisition: C.V., M.Cr., C.C and C.G.; All authors read and approved the final manuscript.

CRediT authorship contribution statement

Maria Teresa Golia: Formal analysis, Writing – original draft, Investigation. **Roberto Frigerio:** Formal analysis, Writing – review & editing, Investigation. **Susanna Pucci:** Formal analysis, Writing – review & editing, Investigation. **Francesca Sironi:** Formal analysis, Investigation. **Cassandra Margotta:** Formal analysis, Investigation. **Laura Pasetto:** Formal analysis, Investigation. **Camilla Testori:** Investigation, Resources. **Elena Berrone:** Investigation, Resources. **Francesco Ingravalle:** Investigation, Resources. **Marcella Chiari:** Conceptualization. **Alessandro Gori:** Formal analysis, Investigation. **Roberto Duchi:** Investigation, Resources. **Andrea Perota:** Investigation, Resources, Writing – review & editing. **Luca Bergamaschi:** Investigation, Resources. **Antonio D'Angelo:** Investigation, Resources.

Giulia Cagnotti: Investigation, Resources. **Cesare Galli:** Writing – review & editing, Funding acquisition. **Cristiano Corona:** Funding acquisition, Writing – review & editing. **Valentina Bonetto:** Conceptualization, Writing – review & editing. **Caterina Bendotti:** Conceptualization, Writing – review & editing. **Marina Cretich:** Conceptualization, Funding acquisition, Supervision, Writing – original draft. **Sara Francesca Colombo:** Conceptualization, Supervision, Writing – review & editing. **Claudia Verderio:** Conceptualization, Funding acquisition, Supervision, Writing – original draft.

Declaration of competing interest

The authors declare no conflict of interests.

Data availability

The datasets used and analyzed during the current study are available from the corresponding author on reasonable request.

Acknowledgements

Authors are grateful to Dr. Stefano Morara and Giulia Petrillo for help in some experiments and Dr. Giuseppe Lauria for INTERSLA project coordination.

Appendix A. Supplementary data

Supplementary data to this article can be found online at https://doi.org/10.1016/j.expneurol.2024.114716.

References

Agosta, F., Libera, D.D., Spinelli, E.G., Finardi, A., Canu, E., Bergami, A., et al., 2014. Myeloid microvesicles in cerebrospinal fluid are associated with myelin damage and neuronal loss in mild cognitive impairment and alzheimer disease. Ann. Neurol. 76, 813–825.

Basso, M., Bonetto, V., 2016. Extracellular vesicles and a novel form of communication in the brain. Front. Neurosci. 1, 127 www.frontiersin.org.

Benatar, M., Wuu, J., Andersen, P.M., Bucelli, R.C., Andrews, J.A., Otto, M., et al., 2022. Design of a Randomized, placebo-controlled, phase 3 trial of Tofersen initiated in clinically Presymptomatic SOD1 variant carriers: the ATLAS study. Neurotherapeutics. 19, 1248.

Bianco, F., Pravettoni, E., Colombo, A., Schenk, U., Möller, T., Matteoli, M., et al., 2005. Astrocyte-derived ATP induces vesicle shedding and IL-1β release from microglia. J. Immunol. 174, 7268–7277.

Bonfanti, E., Bonifacino, T., Raffaele, S., Milanese, M., Morgante, E., Bonanno, G., et al., 2020. Abnormal upregulation of GPR17 receptor contributes to oligodendrocyte dysfunction in SOD1 G93A mice. Int. J. Mol. Sci. 21 (7), 2395.

Cai, Z.Y., Xiao, M., Quazi, S., Ke, Z.Y., 2018. Exosomes: a novel therapeutic target for Alzheimer's disease? Neural Regen. Res. 13, 930.

Chen, Y., Wu, H., Wang, S., Koito, H., Li, J., Ye, F., et al., 2009. The oligodendrocyte-specific G-protein coupled receptor GPR17 is a cell-intrinsic timer of myelination. Nat. Neurosci. 12, 1398–1406.

Chiaradia, E., Tancini, B., Emiliani, C., Delo, F., Pellegrino, R.M., Tognoloni, A., et al., 2021. Extracellular vesicles under oxidative stress conditions: biological properties and physiological roles. Cells. 10, 1763.

Chieppa, M.N., Perota, A., Corona, C., Grindatto, A., Lagutina, I., Vallino Costassa, E., et al., 2014. Modeling amyotrophic lateral sclerosis in hSOD1 G93A transgenic swine. Neurodegener. Dis. 13, 246–254.

Ciana, P., Fumagalli, M., Trincavelli, M.L., Verderio, C., Rosa, P., Lecca, D., et al., 2006. The orphan receptor GPR17 identified as a new dual uracil nucleotides/cysteinyl-leukotrienes receptor. EMBO J. 25, 4615.

Coleman, B.M., Hill, A.F., 2015. Extracellular vesicles – their role in the packaging and spread of misfolded proteins associated with neurodegenerative diseases. Semin. Cell Dev. Biol. 40, 89–96.

Colombo, E., Borgiani, B., Verderio, C., Furlan, R., 2012. Microvesicles: novel biomarkers for neurological disorders. Front. Physiol. 3, 63.

Crociara, P., Chieppa, M.N., Vallino Costassa, E., Berrone, E., Gallo, M., Lo Faro, M., et al., 2019. Motor neuron degeneration, severe myopathy and TDP-43 increase in a transgenic pig model of SOD1-linked familiar ALS. Neurobiol. Dis. 124, 263–275.

Doyle, L.M., Wang, M.Z., 2019. Overview of extracellular vesicles, their origin, composition, purpose, and methods for exosome isolation and analysis. Cells. 8 (7), 727.

Ekström, K., Crescitelli, R., Pétursson, H.I., Johansson, J., Lässer, C., Bagge, R.O., 2022. Characterization of surface markers on extracellular vesicles isolated from lymphatic exudate from patients with breast cancer. BMC Cancer 22, 1–17.

Fauré, J., Lachenal, G., Court, M., Hirrlinger, J., Chatellard-Causse, C., Blot, B., et al., 2006. Exosomes are released by cultured cortical neurones. Mol. Cell. Neurosci. 31, 642–648.

Ferrara, D., Pasetto, L., Bonetto, V., Basso, M., 2018. Role of extracellular vesicles in amyotrophic lateral sclerosis. Front. Neurosci. 12, 574.

Fiandaca, M.S., Kapogiannis, D., Mapstone, M., Boxer, A., Eitan, E., Schwartz, J.B., et al., 2015. Identification of pre-clinical Alzheimer's disease by a profile of pathogenic proteins in neurally-derived blood exosomes: a case-control study. Alzheimers Dement. 11, 600–607.

Frigerio, R., Musicò, A., Strada, A., Bergamaschi, G., Panella, S., Grange, C., et al., 2022. Comparing digital detection platforms in high sensitivity immune-phenotyping of extracellular vesicles. J. Extracell. Biol. 1, e53.

Fumagalli, M., Daniele, S., Lecca, D., Lee, P.R., Parravicini, C., Douglas, R., et al., 2011. Phenotypic changes, signaling pathway, and functional correlates of GPR17-expressing neural precursor cells during oligodendrocyte differentiation. J. Biol. Chem. 286 (12), 10593–10604.

Gabrielli, M., Raffaele, S., Fumagalli, M., Verderio, C., 2022. The multiple faces of extracellular vesicles released by microglia: where are we 10 years after? Front. Cell. Neurosci. 16, 984690.

Goetzl, E.J., Mustapic, M., Kapogiannis, D., Eitan, E., Lobach, I.V., Goetzl, L., et al., 2016. Cargo proteins of plasma astrocyte-derived exosomes in Alzheimer's disease. FASEB J. 30 (11), 3853–3859.

Goldman, D., Brenner, H.R., Heinemann, S., 1988. Acetylcholine receptor α-, β-, γ-, and δ-subunit mRNA levels are regulated by muscle activity. Neuron 1, 329–333. Cell Press.

Gori, A., Romanato, A., Greta, B., Strada, A., Gagni, P., Frigerio, R., et al., 2020. Membrane-binding peptides for extracellular vesicles on-chip analysis. J. Extracell. Vesicles. 9 (1), 1751428.

Hardiman, O., Al-Chalabi, A., Chio, A., Corr, E.M., Logroscino, G., Robberecht, W., et al., 2017. Amyotrophic lateral sclerosis. Nat. Rev. Dis. Prim. 3, 1–19.

Janas, A.M., Sapoń, K., Janas, T., Stowell, M.H.B., Janas, T., 2016. Exosomes and other extracellular vesicles in neural cells and neurodegenerative diseases. Biochim. Biophys. Acta Biomembr. 1858, 1139–1151.

Kang, S.H., Li, Y., Fukaya, M., Lorenzini, I., Cleveland, D.W., Ostrow, L.W., et al., 2013. Degeneration and impaired regeneration of gray matter oligodendrocytes in amyotrophic lateral sclerosis. Nat. Neurosci. 16, 571–579.

Keren-Shaul, H., Spinrad, A., Weiner, A., Matcovitch-Natan, O., Dvir-Szternfeld, R., Ulland, T.K., et al., 2017. A unique microglia type associated with restricting development of Alzheimer's disease. Cell. Cell 169, 1276–1290.e17.

Krämer-Albers, E.M., Bretz, N., Tenzer, S., Winterstein, C., Möbius, W., Berger, H., et al., 2007. Oligodendrocytes secrete exosomes containing major myelin and stress-protective proteins: trophic support for axons? Proteomics Clin. Appl. 1, 1446–1461.

Lachenal, G., Pernet-Gallay, K., Chivet, M., Hemming, F.J., Belly, A., Bodon, G., et al., 2011. Release of exosomes from differentiated neurons and its regulation by synaptic glutamatergic activity. Mol. Cell. Neurosci. 46, 409–418.

Lasiene, J., Yamanaka, K., 2011. Glial cells in amyotrophic lateral sclerosis. Neurol. Res. Int. 2011, 718987.

Maas, S.L.N., Breakefield, X.O., Weaver, A.M., 2017. Extracellular vesicles: unique intercellular delivery vehicles. Trends Cell Biol. 27, 172–188.

Margotta, C., Fabbrizio, P., Ceccanti, M., Cambieri, C., Ruffolo, G., D'Agostino, J., et al., 2023. Immune-mediated myogenesis and acetylcholine receptor clustering promote a slow disease progression in ALS mouse models. Inflamm Regen. 43.

Philips, T., Rothstein, J.D., 2015. Rodent models of amyotrophic lateral sclerosis. Curr. Protoc. Pharmacol. 69, 5.67.1–5.67.21.

Philips, T., Bento-Abreu, A., Nonneman, A., Haeck, W., Staats, K., Geelen, V., et al., 2013. Oligodendrocyte dysfunction in the pathogenesis of amyotrophic lateral sclerosis. Brain. 136 (Pt 2), 471–482.

Rosen, D.R., Siddique, T., Patterson, D., Figlewicz, D.A., Sapp, P., Hentati, A., et al., 1993. Mutations in cu/Zn superoxide dismutase gene are associated with familial amyotrophic lateral sclerosis. Nature. 364 (6435), 362.

Saint-Pol, J., Gosselet, F., Duban-Deweer, S., Pottiez, G., Karamanos, Y., 2020. Targeting and crossing the blood-brain barrier with extracellular vesicles. Cells. 9, 851.

Scaroni, F., Visconte, C., Serpente, M., Golia, M.T., Gabrielli, M., Huiskamp, M., et al., 2022. miR-150-5p and let-7b-5p in blood myeloid extracellularvesicles track cognitive symptoms in patients withmultiple sclerosis, 11 (9), 1551.

Schomberg, D.T., Tellez, A., Meudt, J.J., Brady, D.A., Dillon, K.N., Arowolo, F.K., et al., 2016. Miniature swine for preclinical modeling of complexities of human disease for translational scientific discovery and accelerated development of therapies and medical devices. Toxicol. Pathol. 44, 299–314.

Seelig, H.P., Schranz, P., Schröter, H., Wiemann, C., Renz, M., 1994. Macrogolgin—a new 376 kD Golgi complex outer membrane protein as target of antibodies in patients with rheumatic disease and HIV infections. J. Autoimmun. Academic Press 7, 67–91.

Silverman, J.M., Fernando, S.M., Grad, L.I., Hill, A.F., Turner, B.J., Yerbury, J.J., et al., 2016. Disease mechanisms in ALS: misfolded SOD1 transferred through exosome-dependent and exosome-independent pathways. Cell. Mol. Neurobiol. 36, 377–381.

Silverman, J.M., Christy, D., Shyu, C.C., Moon, K.-M., Fernando, S., Gidden, Z., et al., 2019. CNS-derived extracellular vesicles from superoxide dismutase 1 (SOD1) G93A ALS mice originate from astrocytes and neurons and carry misfolded SOD1. J. Biol. Chem. 294, 3744–3759.

Talbot, K., 2014. Amyotrophic lateral sclerosis: cell vulnerability or system vulnerability? J. Anat. 224 (1), 45–51.

Tamura, Y., Kataoka, Y., Cui, Y., Takamori, Y., Watanabe, Y., Yamada, H., 2007. Intracellular translocation of glutathione S-transferase pi during oligodendrocyte differentiation in adult rat cerebral cortex in vivo. Neuroscience. 148, 535–540.

Théry, C., Witwer, K.W., Aikawa, E., Alcaraz, M.J., Anderson, J.D., Andriantsitohaina, R., et al., 2018. Minimal information for studies of extracellular vesicles 2018 (MISEV2018): a position statement of the International Society for Extracellular Vesicles and update of the MISEV2014 guidelines. J. Extracell. Vesicles. 7, 1535750.
Turner, B.J., Talbot, K., 2008. Transgenics, toxicity and therapeutics in rodent models of mutant SOD1-mediated familial ALS. Prog. Neurobiol. 85, 94–134.
Verderio, C., Muzio, L., Turola, E., Bergami, A., Novellino, L., Ruffini, F., et al., 2012. Myeloid microvesicles are a marker and therapeutic target for neuroinflammation. Ann. Neurol. 72, 610–624.
Visconte, C., Golia, M.T., Fenoglio, C., Serpente, M., Gabrielli, M., Arcaro, M., et al., 2023. Plasma microglial-derived extracellular vesicles are increased in frail patients with mild cognitive impairment and exert a neurotoxic effect. GeroScience 2023, 1–15.
Yang, H., Wang, G., Sun, H., Shu, R., Liu, T., Wang, C.-E., et al., 2014. Species-dependent neuropathology in transgenic SOD1 pigs. Cell Res. 24, 464–481.
Yin, Y., Chen, H., Wang, Y., Zhang, L., Wang, X., Xipeng, Wang C., 2021. Roles of extracellular vesicles in the aging microenvironment and age-related diseases, 10 (12), e12154.
Zucchi, E., Bonetto, V., Sorarù, G., Martinelli, I., Parchi, P., Liguori, R., et al., 2020. Neurofilaments in motor neuron disorders: towards promising diagnostic and prognostic biomarkers. Mol. Neurodegener. 15.